ARMY RESEARCH LABORATORY

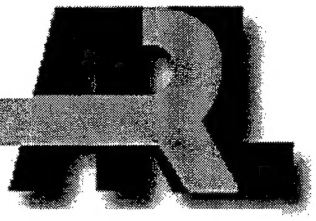

Computational Fluid Dynamics (CFD) Computations With Zonal Navier-Stokes Flow Solver (ZNSFLOW) Common High Performance Computing Scalable Software Initiative (CHSSI) Software

Harris L. Edge
Jubaraj Sahu
Walter B. Sturek
Daniel M. Pressel
Karen R. Heavey
Paul Weinacht
Csaba K. Zoltani
Jerry Clarke
Marek Behr

ARL-TR-1987 JUNE 1999

Army Research Laboratory
Aberdeen Proving Ground, MD 21005-5066

ARL-TR-1987 June 1999

Computational Fluid Dynamics (CFD) Computations With Zonal Navier-Stokes Flow Solver (ZNSFLOW) Common High Performance Computing Scalable Software Initiative (CHSSI) Software

Harris L. Edge
Jubaraj Sahu
Karen R. Heavey
Paul Weinacht
Weapons & Materials Research Directorate, ARL

Walter B. Sturek
Daniel M. Pressl
Csaba K. Zoltani
Corporate Information & Computing Directorate, ARL

Jerry Clarke
Raytheon Systems Company

Marek Behr
U.S. Army High Performance Computing Research Center

Abstract

This report presents an overview of the software developed under the common high performance computing scalable software initiative (CHSSI), computational fluid dynamics (CFD) 6 project. Under the project, a proven zonal Navier-Stokes solver was rewritten for scalable parallel performance on both shared memory and distributed memory high performance computers. At the same time, a graphical user interface (GUI) was developed to help the user set up the problem, provide real-time visualization, and execute the solver. The GUI is not just an input interface but provides an environment for the systematic, coherent execution of the solver, thus making it a more useful, quicker and easier application tool for engineers. Also part of the CHSSI project is a demonstration of the developed software on complex applications of interest to the Department of Defense. Results from computations of 10 brilliant anti-armor (BAT) submunitions simultaneously ejecting from a single Army tactical missile and a guided multiple launch rocket system missile are discussed. Experimental data were available for comparison with the BAT computations. The CFD computations and the experimental data show good agreement and serve as validation for the accuracy of the solver.

ACKNOWLEDGMENTS

The authors would like to thank the U.S. Army Research Laboratory Major Shared Research Center at Aberdeen Proving Ground, Maryland, for the use of their computing resources.

INTENTIONALLY LEFT BLANK

TABLE OF CONTENTS

INTENTIONALLY LEFT BLANK

LIST OF FIGURES

INTENTIONALLY LEFT BLANK

COMPUTATIONAL FLUID DYNAMICS (CFD) COMPUTATIONS WITH ZONAL NAVIER-STOKES FLOW SOLVER (ZNSFLOW) COMMON HIGH PERFORMANCE COMPUTING SCALABLE SOFTWARE INITIATIVE (CHSSI) SOFTWARE

1. INTRODUCTION

The thrust of the work described here is to further develop an existing computational fluid dynamics (CFD) code and make it more accessible for engineers. The code was developed as part of the common high performance computing scalable software initiative (CHSSI) and is now called the zonal Navier-Stokes flow solver (ZNSFLOW). ZNSFLOW is actually a suite of codes that basically includes a zonal Navier-Stokes solver and graphical user interface (GUI) environment for problem setup, interactive visualization, and solver execution. The primary goals of the ZNSFLOW CHSSI project are to

1. Develop a scalable version of a zonal Navier-Stokes solver;

2. Add features to the ZNSFLOW software which allow general applicability and ease of use; and

3. Demonstrate the design utility of the scalable ZNSFLOW software by solving current Department of Defense (DoD) priority viscous flow problems.

In keeping with these goals, the report gives a broad overview of the ZNSFLOW CHSSI project, the ZNSFLOW solver and its capabilities, as well as the GUI environment. Some results from test cases are presented to demonstrate recent applications of ZNSFLOW.

2. THE ZNSFLOW SOLVER

The ZNSFLOW solver originally was known as F3D, a fully vectorized Formula Translator (FORTRAN) 77 code used on Cray vector computers such as the C90.**[1,2]** During the CHSSI program, the code has been rewritten to provide scalable performance on a number of computer architectures. Other added enhancements include dynamic memory allocation and highly optimized cache management. Aside from the performance aspects, the solver has been provided with a number of enhancements to make it more user friendly and capable of performing flow field computations for complex configurations of interest to DoD. The solver was written to operate with and without a GUI environment. A large portion of the effort spent on the ZNSFLOW CHSSI project went toward increasing ease of use and general applicability of the ZNSFLOW solver. The distributed interactive computing environment (DICE) GUI allows some

of the ZNSFLOW solver's more complex features to be easily employed. For example, the solver allows for one-to-one overlaps between grid zones in any direction. The GUI makes the setup for this generalized data exchange intuitive and also provides some simple error-checking capabilities to catch mistakes in creating the input file. Many of the boundary conditions are generalized and can be applied to any surface or line.

In addition, the solver can perform computations with the chimera composite grid discretization technique.**[3-5]** By using the chimera technique, one can greatly simplify the grid topology and grid generation for very complex systems. One of the drawbacks in using the chimera technique has been the increased complexity and corresponding confusion in applying a turbulence model. A chimera model can be composed of multiple zones, with each zone possibly having a unique grid topology. Most turbulence models have specific directional, orientation, or distance-related requirements for correct application. For a complex chimera model, applying a turbulence model can be a very complex process. This problem has been addressed in ZNSFLOW by installing a pointwise turbulence model **[6]** that is not orientation specific. This greatly simplifies the setup of the turbulence model. Wall location information is supplied when the wall boundary conditions are set by the user through the GUI. Currently, a Baldwin-Lomax **[7]** and a one-equation pointwise turbulence model have been validated. A two-equation pointwise turbulence model is undergoing testing.

The ZNSFLOW software has been targeted to operate on both shared memory and distributed memory architectures. In order to fulfill the CHSSI program requirement that the ZNSFLOW solver be scalable on applicable computers, it was decided to create two versions of the ZNSFLOW solver, with one version optimized to operate on shared memory architectures and the other optimized to operate on distributed memory architectures. The shared memory version of the solver employs loop-level parallelism that has highly optimized cache management. The distributed memory version is not as fully developed as the shared memory version. The distributed memory solver currently uses the shared memory (SHMEM) library for the Cray T3E and Origin 2000 computers and the message-passing interface (MPI) library for the IBM® SP® computer. Either current library can be chosen with conditional compiler switches. Once the ZNSFLOW software is complete, the differences between the multiple versions of the solver should be transparent to the user. Both versions of the ZNSFLOW solver apply the same unsteady Reynolds averaged thin layer Navier-Stokes equations to compute flow field solutions with no changes in the time-tested solution algorithm.

2.1 Governing Equations and Solution Technique

The complete set of time-dependent, Reynolds-averaged, thin layer, Navier-Stokes equations is solved numerically to obtain a solution to this problem. The numerical technique used is an implicit, finite difference scheme. Steady state calculations are made to numerically compute the flow field.

2.1.1 *Governing Equations*

The complete set of three-dimensional (3D), time-dependent, generalized geometry, Reynolds-averaged, thin layer, Navier-Stokes equations for general spatial coordinates ξ, η, and ζ can be written as follows (Pulliam & Steger 1982):

$$\partial_\tau \hat{q} + \partial_\xi \hat{F} + \partial_\eta \hat{G} + \partial_\zeta \hat{H} = Re^{-1} \partial_\zeta \hat{S}, \tag{1}$$

in which

$\xi = \xi(x, y, z, t)$ - longitudinal coordinate;
$\eta = \eta(x, y, z, t)$ - circumferential coordinate;
$\zeta = \zeta(x, y, z, t)$ - nearly normal coordinate;
$\tau = t$ - time

In Equation (1), $\hat{q}$ contains the dependent variables (density, three velocity components, and the energy), and $\hat{F}, \hat{G}$, and $\hat{H}$ are flux vectors. The thin layer approximation is used here, and the viscous terms involving velocity gradients in both the longitudinal and circumferential directions are neglected. The viscous terms are retained in the normal direction, ζ, and are collected into the vector $\hat{S}$. In the wake or the base region, similar viscous terms are also added in the stream-wise direction, ξ. For computation of turbulent flows, the turbulent contributions are supplied through an algebraic eddy viscosity turbulence model developed by Baldwin and Lomax **[7]** or a pointwise turbulence model **[6]**.

2.1.2 *Numerical Technique*

The implicit, approximately factored scheme for the thin layer, Navier-Stokes equations using central differencing in the η and ζ directions and an upwind scheme in ξ is written in the following form **[2]**:

$$\left[I + i_b h \delta_\xi^b \left(\hat{A}^+ \right)^n + i_b h \delta_\zeta \hat{C}^n - i_b h \, Re^{-1} \overline{\delta}_\zeta J^{-1} \hat{M}^n J - i_b D_i |_\zeta \right] \times$$

$$\left[I + i_b h \delta_\xi^f \left(\hat{A}^- \right)^n + i_b h \delta_\eta \hat{B}^n - i_b D_i |_\eta \right] \Delta \hat{Q}^n =$$

$$i_b \Delta t \left\{ \delta_\xi^b \left[\left(\hat{F}^+ \right)^n - \hat{F}_\infty^+ \right] + \delta_\xi^f \left[\left(\hat{F}^- \right)^n - \hat{F}_\infty^- \right] + \delta_\eta \left[\hat{G}^n - \hat{G}_\infty \right] + \delta_\zeta \left[\hat{H}^n - \hat{H}_\infty \right] - Re^{-1} \overline{\delta}_\zeta \left[\hat{S}^n - \hat{S}_\infty \right] \right\} -$$

$$i_b D_e \left(\hat{Q}^n - \hat{Q}_\infty \right), \tag{2}$$

in which h = Δt or (Δt)/2. The free-stream fluxes are subtracted from the governing equation to reduce the possibility of error from the free-stream solution corrupting the converged solution. Here, δ is typically a three-point, second order, accurate central difference operator; $\overline{\delta}$ is a midpoint operator used with the viscous terms; and the operators δ_ξ^b and δ_ξ^f are backward and forward three-point difference operators. The flux $\hat{F}$ has been eigensplit and the matrices $\hat{A}, \hat{B}, \hat{C}$, and $\hat{M}$ result from local linearization of the fluxes about the previous time level. Here, J denotes the Jacobian of the coordinate transformation. Dissipation operators D_e and D_i are used in the central space differencing directions. The smoothing terms used in the present study are of the form

$$D_e|_\eta = (\Delta t) J^{-1} \left[\varepsilon_2 \overline{\delta} \rho(B) \beta \overline{\delta} + \varepsilon_4 \overline{\delta} \, \frac{\rho(B)}{1+\beta} \overline{\delta}^3 \right] |_\eta \, J,$$

and

$$D_i|_\eta = (\Delta t) J^{-1} \left[\varepsilon_2 \overline{\delta} \rho(B) \beta \overline{\delta} + 2.5 \varepsilon_4 \overline{\delta} \rho(B) \overline{\delta} \right] |_\eta \, J,$$

in which

$$\beta = \frac{\left| \overline{\delta}^2 P \right|}{\left| \left(1 + \delta^2 \right) P \right|},$$

and ρ(B) is the true spectral radius of B. The idea here is that the fourth difference will be tuned down near shocks (e.g., as β gets large, the weight on the fourth difference drops down while the second difference tunes up).

2.2 Chimera Composite Grid Scheme

The chimera overset grid technique greatly adds to the number of applications to which the ZNSFLOW solver can be applied. The chimera overset grid technique, which is ideally suited to multi-body problems, **[8-10]** involves generating independent grids about each body and then oversetting them onto a base grid to form the complete model. This procedure reduces a complex

multi-body problem into a number of simpler subproblems. An advantage of the overset grid technique is that it allows computational grids to be obtained for each body component separately and thus makes the grid generation process easier. Because each component grid is generated independently, portions of one grid may lie within a solid boundary contained within another grid. Such points lie outside the computational domain and are excluded from the solution process. Equation 2 has been modified for chimera overset grids by the introduction of the flag i_b to achieve just that. This i_b array accommodates the possibility of having arbitrary holes in the grid. The i_b array is defined so that $i_b = 1$ at normal grid points and $i_b = 0$ at hole points. Thus, when $i_b = 1$, Equation 2 becomes the standard scheme, but when $i_b = 0$, the algorithm reduces to $\Delta\hat{Q}^n = 0$ or $\hat{Q}^{n+1} = \hat{Q}^n$, leaving $\hat{Q}$ unchanged at hole points. The set of grid points that forms the border between the hole points and the normal field points is called inter-grid boundary points. These points are updated by interpolating the solution from the overset grid that created the hole. Values of the i_b array and the interpolation coefficients needed for this update are provided by a separate algorithm.**[3]**

Figure 1 shows an example where the parent missile grid is a major grid and the brilliant anti-armor (BAT) submunition grid is a minor grid. The submunition grid is completely overlapped by the missile grid, and thus its outer boundary can obtain information by interpolation from the missile grid. Similar data transfer or communication is needed from the submunition grid to the missile grid. However, a natural outer boundary that overlaps the submunition grid does not exist for the missile grid. The overset grid technique creates an artificial boundary or a hole boundary within the missile grid that provides the required path for information transfer from the submunition grid to the missile grid. The resulting hole region is excluded from the flow field solution in the missile grid.

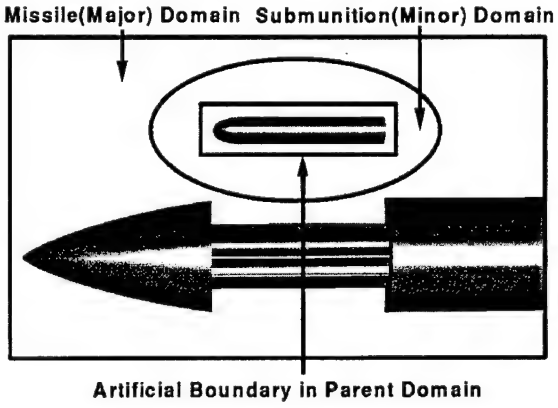

Figure 1. Inter-grid Communications.

3. THE DISTRIBUTED INTERACTIVE COMPUTING ENVIRONMENT

As stated earlier, ZNSFLOW is a suite of codes. Part of that suite is DICE.**[11]** At present, only the shared memory solver has been integrated into DICE. DICE provides a GUI that allows a user to create an input file for the ZNSFLOW solver. DICE can also be used to execute the ZNSFLOW solver once the input file has been created. In addition, once the solver is executing, DICE can provide real-time visualization of the flow field as it is being computed. Even if the execution of the solver was initiated from a previous day, DICE allows the user to connect to the application on a remote computer and visually monitor its progress on a local workstation. DICE provides a number of options for visualizing data. The user can choose surface contours, isosurfaces, x-y plots, or spreadsheets to display the data.

Figure 2 shows some of the GUI windows that a user may access. A flow field visualization window is visible. The user may interactively rotate or translate the object in the window to view the flow field from any position. Beneath the visualization window is the boundary condition setup window. To the right of the boundary condition window is a data directory window. This allows the user to drag and drop specific solver-generated data to DICE utilities such as the isosurface plotter. Farther to the right is the solver execution window. More controls for excuting the solver on multiple platforms are available. To the right of the visualization window is the main interface from which all the other windows are initiated.

It is important to note that DICE is not only a GUI but an environment that includes a heterogeneous distributed memory system called network distributed global memory (NDGM).**[12]** NDGM uses a client-server approach that allows separate distributed applications to access a single contiguous data buffer that may span the memory of several computers. Data within the buffer are stored and accessed using the standardized hierarchical data format (HDF). Data from the solver can be placed into the buffer and accessed in real time through the DICE GUI by the user. DICE has proved to be an exceptional computational environment for high performance computing software and is currently used to support several codes developed under CHSSI in different computational technical areas (CTA).

4. ZNSFLOW DEMONSTRATION CASES

Demonstration cases were chosen to show the capabilities of the ZNSFLOW software. Both of the demonstration problems require viscous Navier-Stokes CFD modeling for accurate flow field solutions. Two demonstration cases were run on a Silicon Graphics Origin 2000 computer. The first of the two cases to be discussed is the guided multiple launch rocket system

(MLRS) missile. The guided MLRS computational model is built to answer questions about the use of canards to perform controlled maneuvers for a missile with wraparound tail fins. A second demonstration case shows the capability of ZNSFLOW to model complex multi-body systems. Computational models were built for computing the flow field about ten brilliant antitank submunitions being ejected from an Army tactical missile (ATACM). The complexity and uniqueness of this type of multi-body problem result from the aerodynamic interference of the individual components, which include three-dimensional (3-D) shock-shock interactions, shock-boundary layer interactions, and highly viscous-dominated separated flow regions.

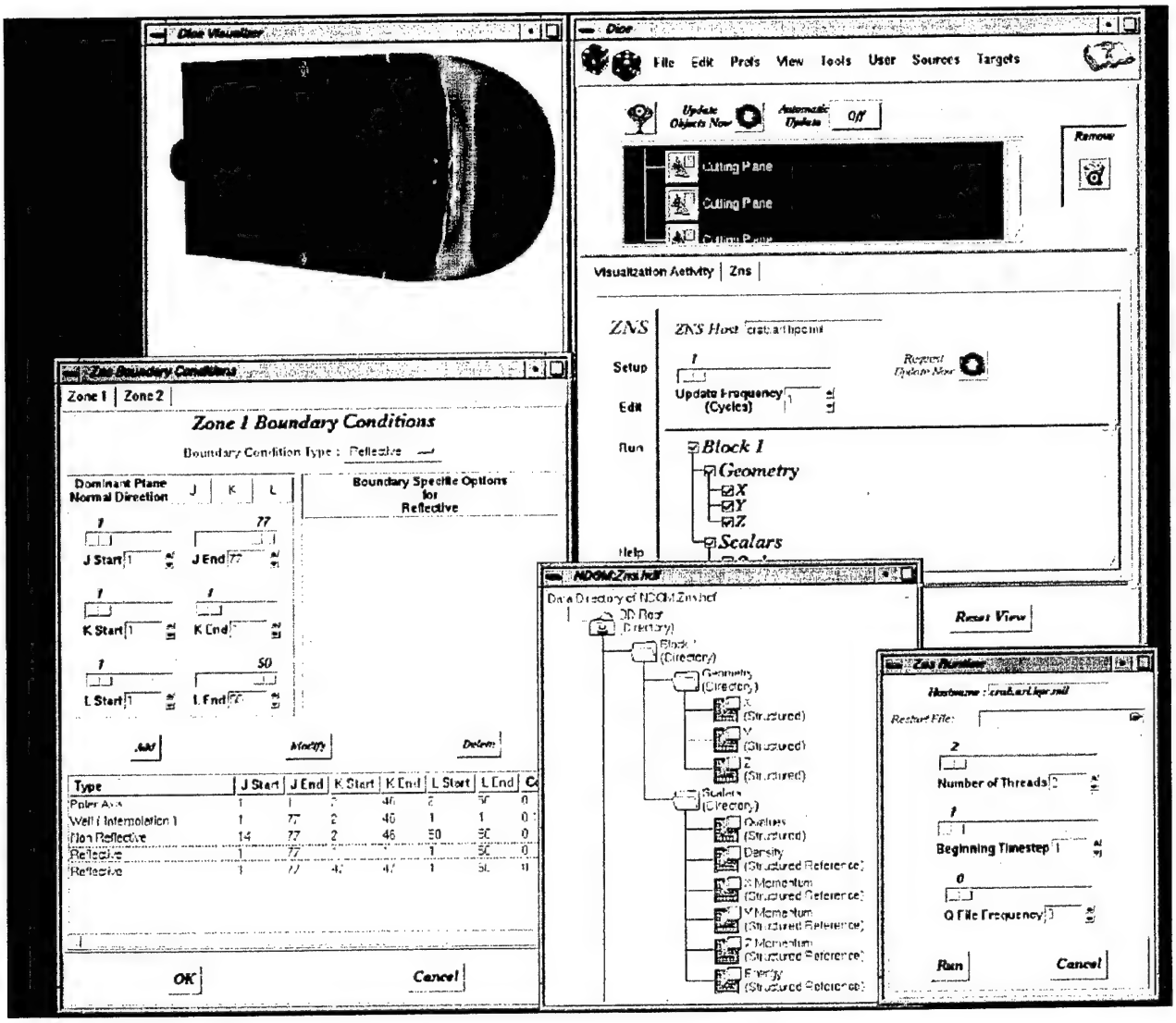

Figure 2. DICE GUI Window.

4.1 Computations for Guided MLRS Missile

The computations will hopefully provide insight for engineers into the interaction of canards with the down-stream wraparound tail fins. Providing control for a missile with wraparound tail fins is more complex than with normal tail fins. The curvature of the wraparound fins allows for easy storage by folding against the missile body while in the launch tube. Immediately after launch, the fins unfold to stabilize to the missile. The cylindrical shape of the wraparound fin is advantageous for packaging, but it can also compromise the dynamic stability of the missile. Wraparound fins have a number of unique aerodynamic traits, the most infamous of which is the roll moment that they generate; this may change in sign and magnitude during the course of a trajectory. The roll moment contributes to the missile spin rate. During the course of flight of a wraparound fin missile, it is possible for the missile's spin rate to increase or decrease more than once. In addition, the direction of spin may change. This type of behavior can produce poor flight dynamics. CFD can be a useful tool for predicting the aerodynamics of wraparound fin missiles.**[13,14]** The information gained from the computations will hopefully aid in a successful design of the guided MLRS and future missiles equipped with wraparound fins.

Initial computations have provided interesting information about the guided MLRS missile flow field. Wind tunnel data are available for comparison. However, because of an error attributable to miscommunication, the nose and canard geometry of the computational model vary slightly from that of the wind tunnel model. The results still provide insight and will demonstrate the capability of ZNSFLOW for providing flow field solutions for this configuration. The computations have been run at 0° angle of attack at velocities of Mach 1.6 and Mach 2.2 and at 10° angle of attack at Mach 1.6. For all computations, each canard has a deflection of 10°. A large computational model, exceeding 24 million grid points, was made for flow field computations of the missile at angle of attack. The computations demonstrated the ability of ZNSFLOW software to handle large data sets. The computational models used for the 0° angle of attack computations exploited symmetry and were one-fourth the size of the computational model used for the angle of attack case.

Figure 3 shows a ZNSFLOW-computed solution of the guided MLRS missile at Mach 1.6 at 0° angle of attack. Figure 4 shows a ZNSFLOW-computed solution of the guided MLRS missile at Mach 1.6 and 10° angle of attack. The flow field changes substantially with the increased angle of attack. Figures 3a and 4a show pressure contours on a plane 1.4 calibers from the nose. This plane is just aft of the canards. The location of the vortices generated by the canard tips can be seen as small, circular low-pressure regions near the canard tips. Figures 3b and 4b are 3.7 calibers from the nose. The flow field at 0° angle of attack is symmetrical, but the flow field for the 10° angle of attack is asymmetrical. Most noticeable is a large low-pressure region on the visible side of the

body. Since the missile is flying at 10° angle of attack, the deflected canard beneath the body directs more air to the visible side of the body. This low-pressure region extends to the rear of the missile and is visible in Figure 4c, which is approximately 14 calibers from the nose and is just in front of the tail fins. Pressure contours in Figure 3c are at the same location as in Figure 4c. Figure 3c again shows the symmetrical flow field at 0° angle of attack in contrast to the asymmetrical flow field generated at 10° angle of attack shown in Figure 4c. In Figure 3c, the light contour shade between the dark contours near the body indicates the locations of the tail fins. The dark pressure contours in Figure 3c indicate that the position of the canard tip vortices is actually between the wraparound tail fins.

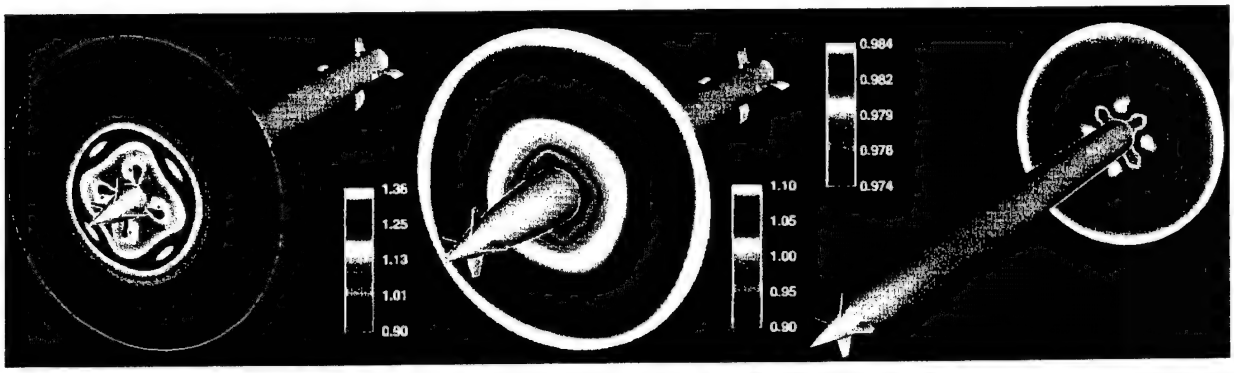

a. 1.4 calibers from nosetip. b. 3.7 calibers from nosetip. c. 14.4 calibers from nosetip.

Figure 3. Normalized Pressure Contours at Mach 1.6 and 0° Angle of Attack.

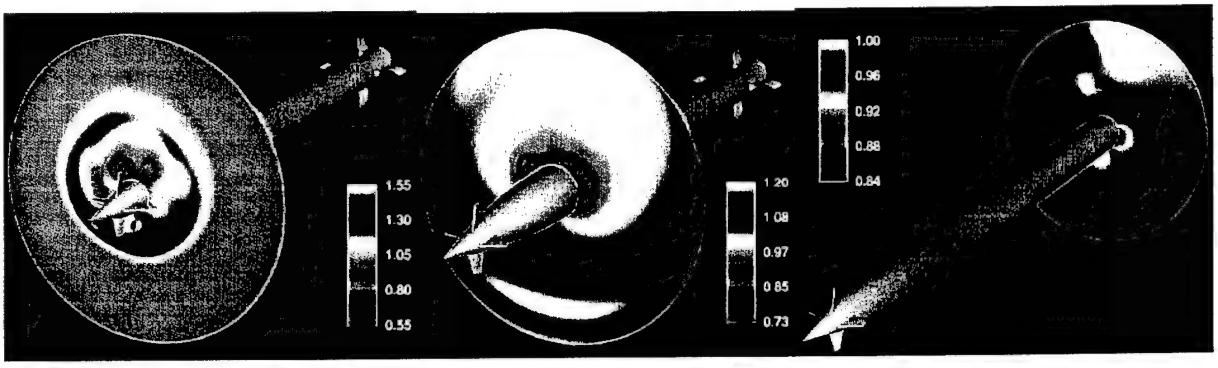

a. 1.4 calibers from nosetip. b. 3.7 calibers from nosetip. c. 14.4 calibers from nosetip.

Figure 4. Normalized Pressure Contours at Mach 1.6 and 10° Angle of Attack.

Visualization using particle traces has also provided some insight to the guided MLRS flow field. Figure 5 shows particle traces released from the wakes of the deflected canards. The

particle traces for Figure 5a were generated from a Mach 1.6 flow field solution, while the particle traces for Figure 5b were generated from a Mach 2.2 solution. Figure 5a and 5b indicate that the flow fields are similar at Mach 1.6 and Mach 2.2 at 0° angle of attack. An interesting note is that particles released at the base of the canards nearly hit the base of the tail fins. However, particles released at the canard tips are caught in a vortex that passes between the fins. The particle traces in Figure 5c are an indication of the differences in the flow field for a guided MLRS missile at 0° and 10° angle of attack. The particle traces for Figure 5c were generated from a Mach 1.6 flow field solution at 10° angle of attack. The traces show that particles released from the canard wakes are swept to the lee side or upper side of the missile body. As mentioned earlier, the canard beneath the missile deflects more air flow to one side of the body, creating a large difference in the flow fields on the sides of the body. For the 10° angle of attack case, only the canard tip on the far side of the body generates a strong vortex. An indication of this vortex is the small dark circle on the left side of the body that is visible in Figure 4b.

4.2 Computations for BAT Submunitions Ejecting From ATACM

The ATACM-BAT multi-body problem involves the radial dispensing of several BAT submunitions (see Figure 6) at a low supersonic speed. This case is ideally suited for the chimera overset grid technique described earlier. The chimera scheme allows each BAT to be modeled with its own simple orthogonal grid as seen in Figure 7. The trajectory of the 3-D radial dispensing submunitions depends on the initial ejection velocity. The flow field is complex and involves 3-D shock-boundary layer interactions and ATACM-to-BAT as well as BAT-to-BAT interactions. Detailed experimental or theoretical data were not available to help evaluate the submunition dispensing phenomenon for the entire BAT system, and thus the numerical solution of this problem was initiated.**[15-17]** The chimera solution procedure was successfully used to help determine the aerodynamic interference effects.**[16]**

For a set of wind tunnel experiments, the position of the submunitions was set in order to evaluate flow field correction factors for nonsymmetrical dispensation at a distance near and far from the bay. The flow field correction factors are used in six-degree-of-freedom simulations of BAT dispensation for different conditions. CFD computations were made for two configurations: Configuration A, which places the submunitions relatively close to the missile bay, and Configuration B, which places them farther away from the turbulence generated by the missile bay. For both Configurations A and B, there is equidistant circumferential spacing for each submunition except one, which has a 5° offset. The submunition with the circumferential offset is located at approxi-

mately the 11 o'clock position. Figure 8 provides a visual reference for the submunition positions for Configurations A and B.

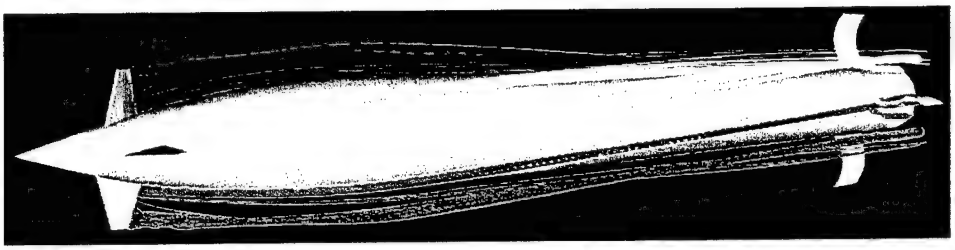

a. Particle traces for Mach 1.6, 0° angle of attack.

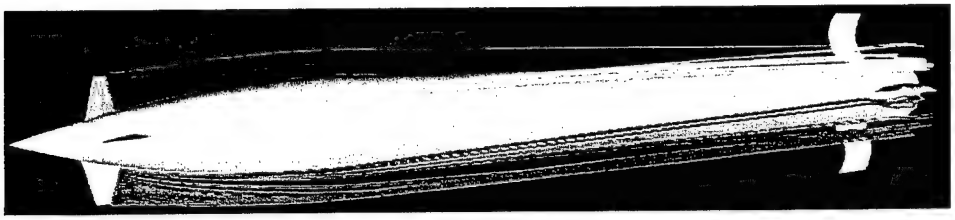

b. Particle traces for Mach 2.2, 0° angle of attack.

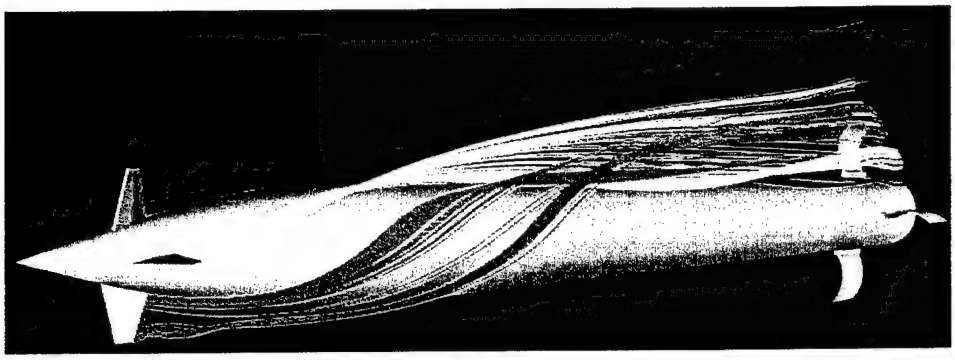

c. Particle traces for Mach 1.6, 10° angle of attack.

Figure 5. Particle Traces at Various Mach Numbers and Angles of Attack.

Surface pressure contours are shown for Configuration A in Figure 9 and for Configuration B in Figure 10. The surface pressures on the Configuration A submunitions reveal much stronger pressure gradients than the submunitions in Configuration B. Also, surface pressure contours within the ATACM missile bay are somewhat different between Configurations A and B. The stronger pressure gradients on the Configuration A submunitions, which are much closer to the ATACM missile bay, are indicative of the higher pitching moments generated, which tend to push the nose of the BAT submunitions radially inward toward the ATACM missile bay. Since the computations include multiple BAT submunitions, BAT-to-BAT interactions are included.

These interactions are critical and have a strong effect on the aerodynamic forces and moments. The normal force and pitching moment coefficients vary between the submunitions, indicating the asymmetrical nature of the interacting flow field.

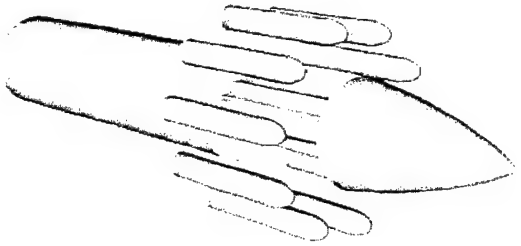

Figure 6. Diagram of the Multi-body System.

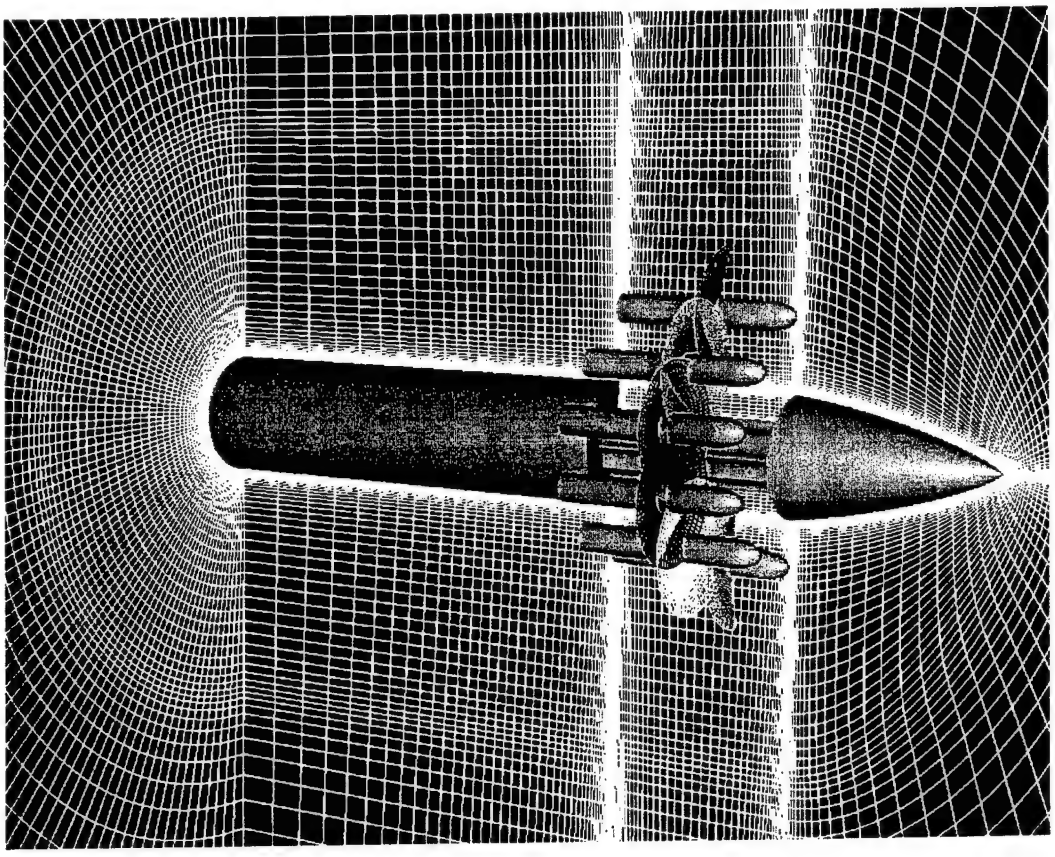

Figure 7. Grids for the BAT Submunition Dispensing From ATACM.

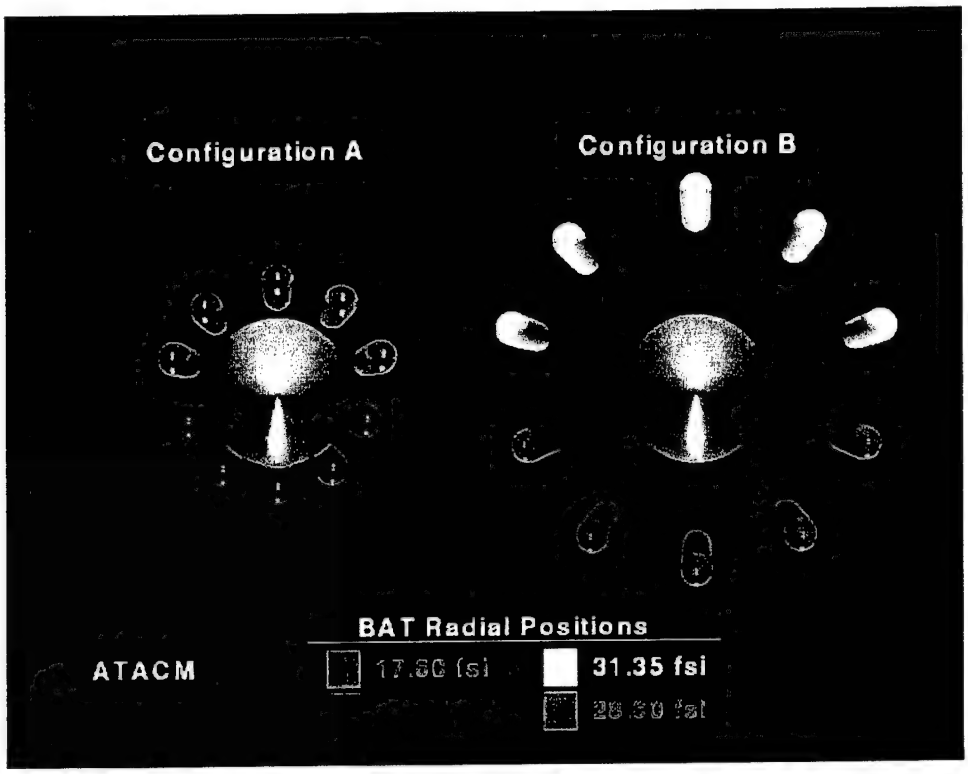

Figure 8. Configuration A and B Submunition Location.

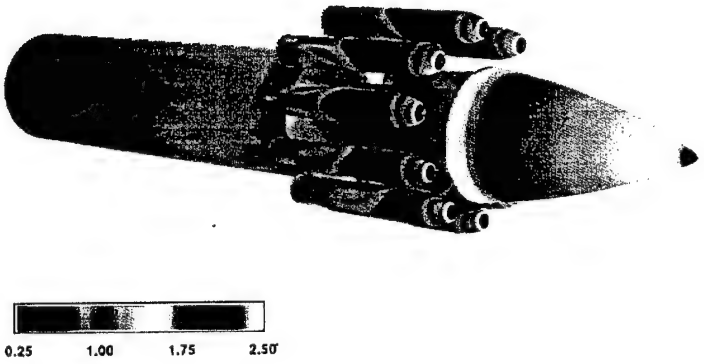

Figure 9. Normalized Surface Pressure Contours for Configuration A.

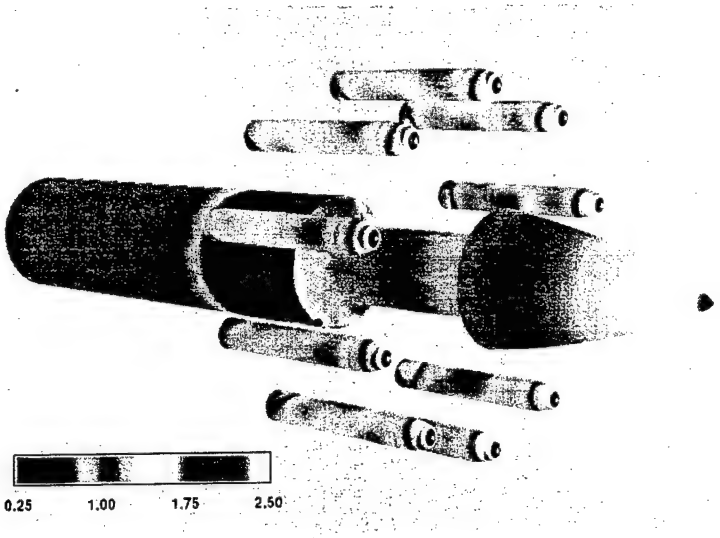

Figure 10. Normalized Surface Pressure Contours for Configuration B.

Some experimental data **[18]** were available for comparison with the computational results of Configuration A. Figure 11 provides a visual reference for location of the BATs that were the source of the experimental data. A BAT at approximately the 5 o'clock position was equipped to record pressure data. Pressure data were collected on the side of the BAT closest to the ATACM and the side facing away from the ATACM. On either side of the BAT, pressure data were taken at five positions. Unfortunately, the pressure data obtained from the experiment on the side of the BAT facing the ATACM do not appear to be accurate. However, the pressure coefficient data computed from the CFD solution on the side of the BAT facing the ATACM are plotted in Figure 12. Figure 13 shows a comparison between the pressure coefficient obtained from experimental and CFD-calculated data on the side of the BAT facing away from the ATACM. Both Figures 12 and 13 show the pressure coefficient as a function of the length of the BAT body where X/L = 0 corresponds to the BAT nose and X/L = 1 corresponds to the end of the BAT body. Figure 13 shows that the pressure coefficient computed from the CFD solution is in very good agreement with experimental data. The CFD-computed data plotted in Figures 12 and 13 provide an interesting comparison that demonstrates the asymmetry of the flow field about the BAT and the strong influence of the ATACM proximity to the BAT. Although the comparison between the experimentally obtained and CFD-computed pressure coefficient is quite good, the comparisons between experimentally obtained and CFD-computed force and moments indicate that some flow field characteristics may not be captured accurately by the CFD solution.

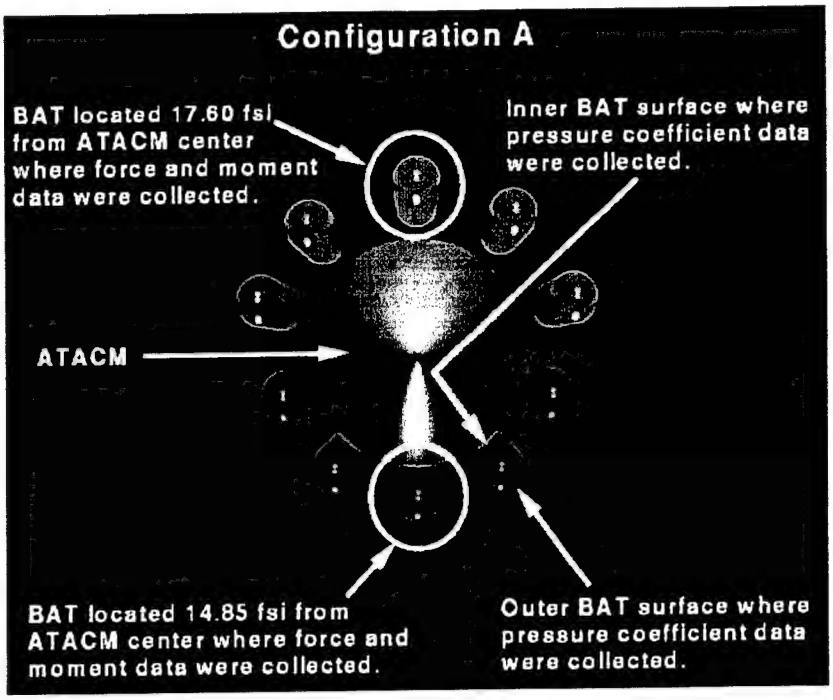

Figure 11. Locations Where Experimental Data Were Collected.

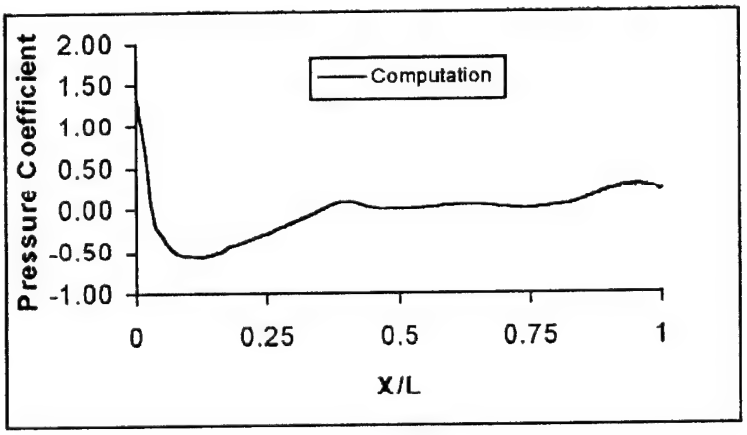

Figure 12. Pressure Coefficient Versus BAT Length for BAT Surface Facing ATACM.

Force and moment data were collected from the BATs located at the 12 o'clock and 6 o'clock positions. The BAT at the 12 o'clock position has a radial distance from the ATACM center of 17.60 full scale inches (fsi). The BAT at the 6 o'clock position has a radial distance from the ATACM center of 14.85 fsi. Figure 14 shows both the experimental data and the data computed from the CFD flow field solution. The data in Figure 14 indicate that the CFD-computed data match the experimental data of the BAT 17.60 fsi from the ATACM center more closely than the experimental and computed data of the BAT 14.85 fsi from the ATACM center.

The data for the normal force, CN, are in good agreement for the BAT 17.60 fsi from the ATACM center. The side force, CY, data appear to be the same for the CFD-computed side force and the experimental side force. This is somewhat misleading because the magnitude of the side force is much smaller than the normal force and pitching moment, Cmz (coefficient of moment about the Z axis). The relatively small side force is a good indication that the BATs are not likely to move closer together when being ejected from the ATACM bay at 0° angle of attack. The difference between the pitching moment for experimental data and CFD-computed data is less for the BAT farthest from the ATACM. This seems to indicate increased difficulty in computing the flow field for the ATACM-BAT multi-body problem accurately when the BATs are almost in the ATACM bay.

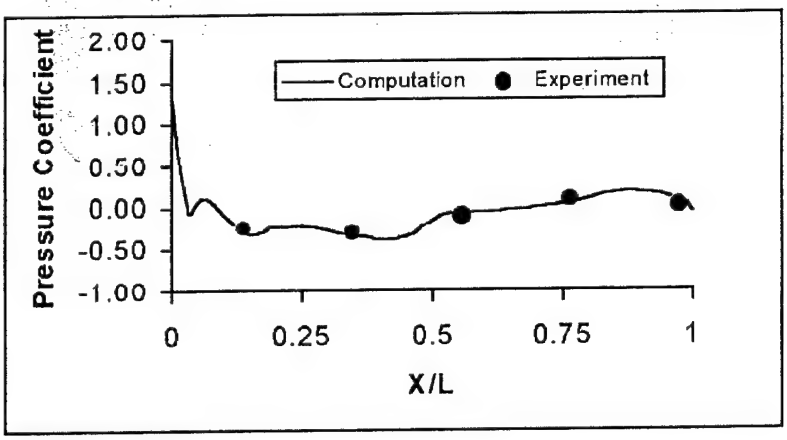

Figure 13. Pressure Coefficient Versus BAT Length for BAT Surface Facing Away From ATACM.

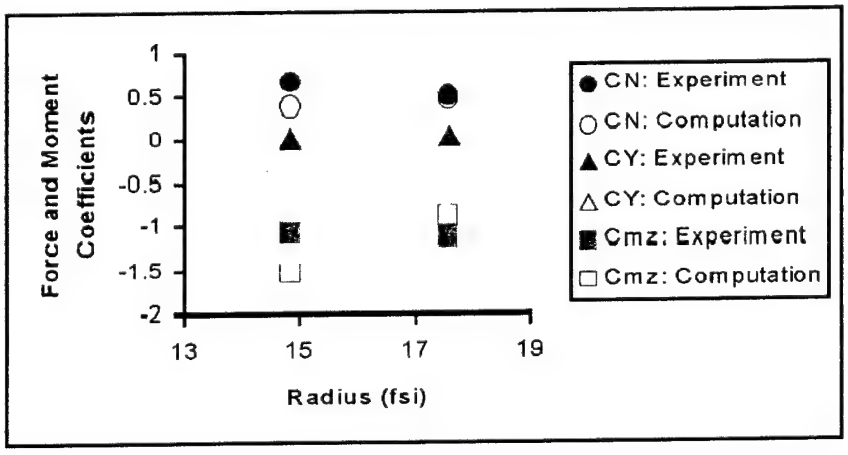

Figure 14. Force and Moment Coefficients for Configuration A.

The drag coefficient computed from the CFD solutions compares very well with the measured drag coefficient. Figure 15 shows a plot for the drag coefficient of the same BATs that were instrumented to obtain the force and moment data displayed in Figure 14. In the experiment, each BAT was mounted on a "sting." The stings were not modeled in the CFD computation. The total drag coefficient was obtained from a force measurement of the BAT with sting. The experimental value of the BAT forebody drag was estimated by taking a pressure measurement near the BAT base and using it to estimate the base drag component of the total drag coefficient. The base drag component was then subtracted from the total drag to obtain the forebody drag. An interesting note is the increase in drag with the increased distance of the BAT from the ATACM center.

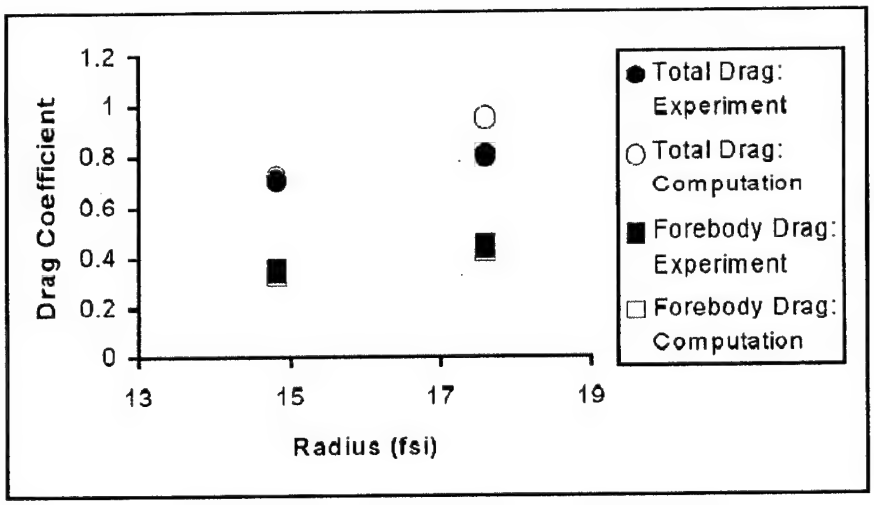

Figure 15. Drag Coefficients for Configuration A.

5. CONCLUDING REMARKS

A broad overview of the software developed under the CHSSI CFD-6 project has been presented. The scalable Navier-Stokes solver executed through the interactive computing environment, DICE, provides enginneers with a fast and comprehensive CFD computation and analysis tool for complex configurations that require large computational resources. However, it can perform computations for simple cases just as well. The software allows the user to perform, monitor, and visualize the computations on large high performance computers without copying the computational mesh and solution to their local workstation. The comprehensive interface provides control for every aspect of the computation. It was also demonstrated that the ZNSFLOW software provides accurate and visually informative results for large complex configurations such as the guided MLRS missile and BAT dispersal from ATACM. The

predictive numerical capability documented allows for accurate computation of flow fields that capture complex aerodynamic phenomena, such as interference effects, required for the improved design and modification of current and future DoD projects.

REFERENCES

1. Pulliam, T.H., and J.L. Steger, "On Implicit Finite-Difference Simulations of Three-Dimensional Flow," AIAA Journal, Vol. 18, No. 2, pp. 159–167, February 1982.

2. Steger, J.L., S.X. Ying, and L.B. Schiff, "A Partially Flux-Split Algorithm for Numerical Simulation of Compressible Inviscid and Viscous Flows," Proceedings of the Workshop on CFD, Institute of Nonlinear Sciences, University of California, Davis, CA, 1986.

3. Steger, J.L., F.C. Dougherty, and J.A. Benek, "A Chimera Grid Scheme," Advances in Grid Generation, edited by K.N. Ghia and U. Ghia, ASME FED-5, June 1983.

4. Benek, J.A., T.L. Donegan, and N.E. Suhs, "Extended Chimera Grid Embedding Scheme With Application to Viscous Flows," AIAA Paper No. 871126CP, 1987.

5. Meakin, R.L., "Computations of the Unsteady Flow About a Generic Wing/Pylon/Finned Store Configuration," AIAA 92-4568-CP, August 1992.

6. Goldberg, U.C., O. Peroomian, S. Chakravarthy, "A Wall-Distance-Free K-E Model With Enhanced Near-Wall Treatment," ASME Journal of Fluids Engineering, Vol. 120, pp. 457-462, 1998.

7. Baldwin, B.L., H. Lomax, "Thin Layer Approximation and Algebraic model for Separated Turbulent Flows," AIAA 78-257, January 1978.

8. Ferry, E.N., J. Sahu, and K.R. Heavey, "Navier-Stokes Computations of Sabot Discard using Chimera Scheme," Proceedings of the 16th International Symposium on Ballistics, September 1996.

9. Sahu, J., K.R. Heavey, and E.N. Ferry, "Computational Fluid Dynamics for Multiple Projectile Configurations." Proceedings of the 3rd Overset Composite Grid and Solution Technology Symposium, Los Alamos, NM, October 1996.

10. Sahu, J., K.R. Heavey, and C.J. Nietubicz, "Time-Dependent Navier-Stokes Computations for Submunitions in Relative Motion." Proceedings of the 6th International Symposium on Computational Fluid Dynamics, Lake Tahoe, NV, September 1995.

11. Clarke, J., C.E. Schmitt, and J.J. Hare, "Developing a Full Featured Application from an Existing Code Using the Distributed Interactive Computing Environment," Proceedings of 1998 DoD HPC User's Group Conference, June 1998.

12. Clarke, J., "Network Distributed Global Memory for Transparent Message Passing on Distributed Networks," ARL-CR-173, U.S. Army Research Laboratory, Aberdeen Proving Ground, MD, 1994.

13. Edge, H., "Computation of the Roll Moment Coefficient for a Projectile With Wraparound Fins," ARL-TR-23, U.S. Army Research Laboratory, Aberdeen Proving Ground, MD, 1992.

14. Patel, N., H. Edge, and J. Clarke, "Three-Dimensional (3-D) large Fluid Flow Computations for U.S. Army Applications on KSR-1, CM-200, CM-5, and Cray C-90," ARL-TR-712, U.S. Army Research Laboratory, Aberdeen Proving Ground, MD, 1995.

15. Wooden, P.A., W.B. Brooks, and J. Sahu, "Calibrating CFD Predictions For Use in Multiple Store Separation Analysis," AIAA Paper No. 98-0754, January 1998.

16. Sahu, J., H.L. Edge, K.R. Heavey, and E. Ferry, "Computational Fluid Dynamics Modeling of Multibody Missile Aerodynamic Interference," Proceedings of the NATO RTO AVT Symposium on Missile Aerodynamics, Sorrento Italy, May 1998.

17. Wooden, P.A., E.R. McQuillen, and W.B. Brooks, "Evaluation of a Simplified Multiple Store Interference Model," AIAA Paper No. 98-2800, June 1998.

18. Lee, P.J., "Analysis Report of Army TACMS Block II Captive Airloads Wind Tunnel Data from HSWT Test 1218," 3-18400/6R-050, Lockheed Martin Vought Systems, Dallas, TX, November 1996.

NO. OF COPIES	ORGANIZATION
2	ADMINISTRATOR DEFENSE TECHNICAL INFO CENTER ATTN DTIC OCP 8725 JOHN J KINGMAN RD STE 0944 FT BELVOIR VA 22060-6218
1	DIRECTOR US ARMY RESEARCH LABORATORY ATTN AMSRL CS AL TA REC MGMT 2800 POWDER MILL RD ADELPHI MD 20783-1197
1	DIRECTOR US ARMY RESEARCH LABORATORY ATTN AMSRL CI LL TECH LIB 2800 POWDER MILL RD ADELPHI MD 207830-1197
1	DIRECTOR US ARMY RESEARCH LABORATORY ATTN AMSRL DD J J ROCCHIO 2800 POWDER MILL RD ADELPHI MD 20783-1197
7	CDR US ARMY ARDEC ATTN AMSTE AET A R DEKLEINE C NG R BOTTICELLI H HUDGINS J GRAU S KAHN W KOENIG PICATINNY ARSENAL NJ 07806-5001
1	CDR US ARMY ARDEC ATTN AMSTE CCH V PAUL VALENTI PICATINNY ARSENAL NJ 07806-5001
1	CDR US ARMY ARDEC ATTN SFAE FAS SD MIKE DEVINE PICATINNY ARSENAL NJ 07806-5001
2	USAF WRIGHT AERONAUTICAL LABS ATTN AFWAL FIMG DR J SHANG MR N E SCAGGS WPAFB OH 45433-6553
3	AIR FORCE ARMAMENT LAB ATTN AFATL/FXA STEPHEN C KORN BRUCE SIMPSON DAVE BELK EGLIN AIR FORCE BASE FL 32542-5434
1	CDR NSWC CODE B40 DR W YANTA DAHLGREN VA 22448-5100

NO. OF COPIES	ORGANIZATION
1	CDR NSWC CODE 420 DR A WARDLAW INDIAN HEAD MD 20640-5035
1	CDR NSWC ATTN DR F MOORE DAHLGREN VA 22448
1	NAVAL AIR WARFARE CENTER ATTN DAVID FINDLAY MS 3 BLDG 2187 PATUXENT RIVER MD 20670
4	DIR NASA LANGLEY RESEARCH CENTER ATTN TECH LIBRARY MR D M BUSHNELL DR M J HEMSCH DR J SOUTH LANGLEY STATION HAMPTON VA 23665
2	ARPA ATTN DR P KEMMEY DR JAMES RICHARDSON 3701 NORTH FAIRFAX DR ARLINGTON VA 22203-1714
7	DIR NASA AMES RESEARCH CENTER MS 227 8 L SCHIFF MS 258 1 T HOLST MS 258 1 D CHAUSSEE MS 258 1 M RAI MS 258 1 P KUTLER MS 258 1 P BUNING MS 258 1 B MEAKIN MOFFETT FIELD CA 94035
2	USMA DEPT OF MECHANICS ATTN LTC ANDREW L DULL M COSTELLO WEST POINT NY 10996
2	UNIV OF CALIFORNIA DAVIS DEPT OF MECHANICAL ENGRG ATTN PROF H A DWYER PROF M HAFEZ DAVIS CA 95616

NO. OF COPIES	ORGANIZATION
1	AEROJET ELECTRONICS PLANT ATTN DANIEL W PILLASCH B170 DEPT 5311 PO BOX 296 1100 WEST HOLLYVALE STREET AZUSA CA 91702
1	MIT TECH LIBRARY 77 MASSACHUSETTS AVE CAMBRIDGE MA 02139
1	GRUMANN AEROSPACE CORP AEROPHYSICS RESEARCH DEPT ATTN DR R E MELNIK BETHPAGE NY 11714
2	MICRO CRAFT INC ATTN DR JOHN BENEK NORMAN SUHS 207 BIG SPRINGS AVE TULLAHOMA TN 37388-0370
1	LANL ATTN MR BILL HOGAN MS G770 LOS ALAMOS NM 87545
1	METACOMP TECHNOLOGIES INC ATTN S R CHAKRAVARTHY 650 S WESTLAKE BLVD SUITE 200 WESTLAKE VILLAGE CA 91362-3804
2	ROCKWELL SCIENCE CENTER ATTN S V RAMAKRISHNAN V V SHANKAR 1049 CAMINO DOS RIOS THOUSAND OAKS CA 91360
1	ADVANCED TECHNOLOGY CTR ARVIN/CALSPAN AERODYNAMICS RESEARCH DEPT ATTN DR M S HOLDEN PO BOX 400 BUFFALO NY 14225
1	UNIV OF ILLINOIS AT URBANA CHAMPAIGN DEPT OF MECH & IND ENGINEERING ATTN DR J C DUTTON URBANA IL 61801

NO. OF COPIES	ORGANIZATION
1	UNIVERSITY OF MARYLAND DEPT OF AEROSPACE ENGRG ATTN DR J D ANDERSON JR COLLEGE PARK MD 20742
1	UNIVERSITY OF NOTRE DAME DEPT OF AERONAUTICAL & MECH ENGRG ATTN PROF T J MUELLER NOTRE DAME IN 46556
1	UNIVERSITY OF TEXAS DEPT OF AEROSPACE ENGRG MECH ATTN DR D S DOLLING AUSTIN TX 78712-1055
1	UNIVERSITY OF DELAWARE DEPT OF MECHANICAL ENGRG ATTN DR JOHN MEAKIN NEWARK DE 19716
4	COMMANDER USAAMCOM ATTN AMSAM RD SS AT ERIC KREEGER GEORGE LANDINGHAM CLARK D MIKKELSON ED VAUGHN REDSTONE ARSENAL AL 35898-5252
4	LOCKHEED MARTIN VOUGHT SYS PO BOX 65003 M/S EM 55 ATTN PERRY WOODEN W B BROOKS JENNIE FOX ED MCQUILLEN DALLAS TX 75265-0003
1	COMMANDER US ARMY TACOM-ARDEC BLDG 162S ATTN AMCPM DS MO PETER J BURKE PICATINNY ARSENAL NJ 07806-5000
	ABERDEEN PROVING GROUND
2	DIRECTOR US ARMY RESEARCH LABORATORY ATTN AMSRL CI LP (TECH LIB) BLDG 305 APG AA
3	CDR US ARMY ARDEC FIRING TABLES BRANCH ATTN R LIESKE R EITMILLER F MIRABELLE BLDG 120

NO. OF COPIES	ORGANIZATION
1	DIR USARL ATTN AMSRL CI C NIETUBICZ BLDG 394
3	DIR USARL ATTN AMSRL CI H D HISLEY D PRESSEL C ZOLTANI BLDG 394
1	DIR USARL ATTN AMSRL CI H W STUREK BLDG 328
2	DIR USARL ATTN AMSRL WM I MAY L JOHNSON BLDG 4600
2	DIR USARL ATTN AMSRL WM B A W HORST JR W CIEPIELLA BLDG 4600
1	DIR USARL ATTN AMSRL WM B E M SCHMIDT BLDG 390A
7	DIR ARL ATTN AMSRL WM BA W D'AMICO F BRANDON T BROWN L BURKE J CONDON B DAVIS M HOLLIS BLDG 4600
20	DIR USARL ATTN AMSRL WM BC P PLOSTINS M BUNDY G COOPER H EDGE (5 cys) J GARNER B GUIDOS K HEAVEY D LYON A MIKHAIL V OSKAY J SAHU K SOENCKSEN D WEBB P WEINACHT S WILKERSON A ZIELINSKI BLDG 390
1	DIR USARL ATTN AMSRL WM BD B FORCH BLDG 4600
2	DIR USARL AMSRL WM BE M NUSCA J DESPIRITO BLDG 390

NO. OF COPIES	ORGANIZATION
1	DIR USARL ATTN AMSRL WM BF J LACETERA BLDG 120
1	DIR USARL ATTN AMSRL WM TB R LOTTERO BLDG 309
	ABSTRACT ONLY
1	DIRECTOR US ARMY RESEARCH LABORATORY ATTN AMSRL CS AL TP TECH PUB BR 2800 POWDER MILL RD ADELPHI MD 20783-1197

INTENTIONALLY LEFT BLANK

REPORT DOCUMENTATION PAGE

Form Approved
OMB No. 0704-0188

1. AGENCY USE ONLY *(Leave blank)*	2. REPORT DATE	3. REPORT TYPE AND DATES COVERED
	June 1999	Final

4. TITLE AND SUBTITLE

Computational Fluid Dynamics (CFD) Computations With Zonal Navier-Stokes Flow Solver (ZNSFLOW) Common High Performance Computing Scalable Software Initiative (CHSSI) Software

5. FUNDING NUMBERS

PR: 1L162628AH80

6. AUTHOR(S)

Edge, H.L.; Sahu, J.; Sturek, W.B.; Pressel, D.M.; Heavey, K.R.; Weinacht, P.; Zoltani, C.K. (all of ARL); Clarke, J. (Raytheon Systems); Behr, M. (U.S. Army HPCRC)

7. PERFORMING ORGANIZATION NAME(S) AND ADDRESS(ES)

U.S. Army Research Laboratory
Weapons & Materials Research Directorate
Aberdeen Proving Ground, MD 21010-5066

8. PERFORMING ORGANIZATION REPORT NUMBER

9. SPONSORING/MONITORING AGENCY NAME(S) AND ADDRESS(ES)

U.S. Army Research Laboratory
Weapons & Materials Research Directorate
Aberdeen Proving Ground, MD 21010-5066

10. SPONSORING/MONITORING AGENCY REPORT NUMBER

ARL-TR-1987

11. SUPPLEMENTARY NOTES

12a. DISTRIBUTION/AVAILABILITY STATEMENT

Approved for public release; distribution is unlimited.

12b. DISTRIBUTION CODE

13. ABSTRACT *(Maximum 200 words)*

This report presents an overview of the software developed under the common high performance computing scalable software initiative (CHSSI), computational fluid dynamics (CFD) 6 project. Under the project, a proven zonal Navier-Stokes solver was rewritten for scalable parallel performance on both shared memory and distributed memory high performance computers. At the same time, a graphical user interface (GUI) was developed to help the user set up the problem, provide real-time visualization, and execute the solver. The GUI is not just an input interface but provides an environment for the systematic, coherent execution of the solver, thus making it a more useful, quicker and easier application tool for engineers. Also part of the CHSSI project is a demonstration of the developed software on complex applications of interest to the Department of Defense. Results from computations of 10 brilliant anti-armor (BAT) submunitions simultaneously ejecting from a single Army tactical missile and a guided multiple launch rocket system missile are discussed. Experimental data were available for comparison with the BAT computations. The CFD computations and the experimental data show good agreement and serve as validation for the accuracy of the solver.

14. SUBJECT TERMS

CHSSI
computational fluid dynamics
high performance computing
missiles
Navier-Stokes

15. NUMBER OF PAGES

30

16. PRICE CODE

17. SECURITY CLASSIFICATION OF REPORT	18. SECURITY CLASSIFICATION OF THIS PAGE	19. SECURITY CLASSIFICATION OF ABSTRACT	20. LIMITATION OF ABSTRACT
Unclassified	Unclassified	Unclassified	